Front. Environ. Sci. Eng. 2023, 17(12): 150
https://doi.org/10.1007/s11783-023-1750-9

RESEARCH ARTICLE

Cleaner geopolymer prepared by co-activation of gasification coal fly ash and steel slag: durability properties and economic assessment

Xian Zhou[1,2], Xia Chen[1], Ziling Peng (✉)[1], Yongmen Zhou[2], Yan Li[2], Wang Jian[2], Zeyu Fan[1], Yuchi Chen (✉)[3]

1 Key Laboratory of Geotechnical Mechanics and Engineering of Ministry of Water Resources, Changjiang River Scientific Research Institute, Wuhan 430010, China
2 Jiangxi Research Center on Hydraulic Structures, Jiangxi Provincial Institute of Water Sciences, Nanchang 330029, China
3 Key Joint Laboratory of Environment Simulation and Pollution Control, School of Environment, Tsinghua University, Beijing 100084, China

HIGHLIGHTS

- Better packing density and higher early strength of SS-rich geopolymer.
- C-S-H and portlandite as the main hydration phase in SS-rich geopolymer.
- Increased Si/Al of geopolymer gel and better long-term performance of SFA-rich geopolymer.
- Low cost of SFA-SS geopolymers concrete.

ARTICLE INFO

Article history:
Received 8 February 2023
Revised 16 May 2023
Accepted 2 June 2023
Available online 20 July 2023

Keywords:
Geopolymer
Shell coal gasification fly ash
Steel slag
Heavy metal
Solidification/stabilization
Durability

GRAPHIC ABSTRACT

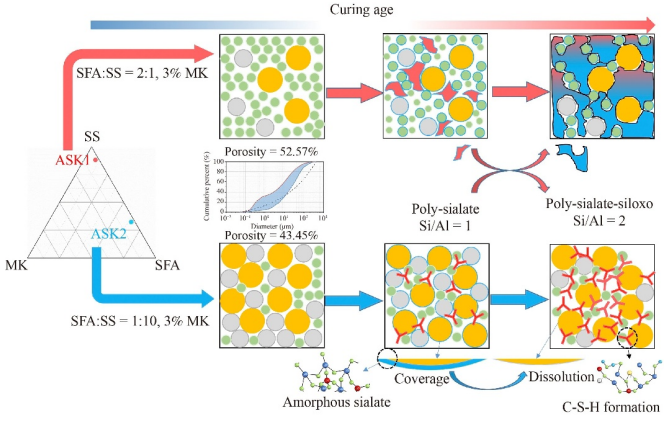

ABSTRACT

Geopolymer is a material with high early strength. However, the insufficient durability properties, such as long-term strength, acid-base resistance, freeze–thaw resistance, leaching toxicity, thermal stability, sulfate resistance and carbonation resistance, restrain its practical application. Herein, a long-term stable geopolymer composite with high final strength (ASK1) was synthesized from shell coal gasification fly ash (SFA) and steel slag (SS). Additionally, a geopolymer composite with high early strength (ASK2) was also synthesized for comparison. The results showed that ASK1 exhibited better performance on freezing-thawing resistance, carbonization resistance and heavy metals stabilization compared to the ASK2 at long-term curing. Raising the curing temperature could accelerate the unconfined compressive strength (UCS) development at initial curing ages of 3 to 7 d. Both ASK1 and ASK2 exhibited excellent acid-base and sulfate corrosion resistance. An increase for UCS was seen under KOH solution and $MgSO_4$ solution corrosion for ASK1. All leaching concentrations of heavy metals out of the two geopolymers were below the standard threshold, even after 50 freezing-thawing cycles. Both ASK1 and ASK2 geopolymer concrete exhibited higher sustainability and economic efficiency than Portland cement concrete. The result of this study not only provides a suitable way for the utilization of industrial solid waste in civil and environmental engineering, but also opens a new approach to improve the long-term stabilities of the geopolymers.

✉ Corresponding authors
E-mails: pengziling0304@163.com (Z. Peng);
glacier@mail.tsinghua.edu.cn (Y. Chen)

1 Introduction

The traditional cementitious material of Portland cement is widely used as a binder material in concrete production. Nevertheless, the cement production process usually leads to significant greenhouse gas emissions and energy consumption, causing severe environmental pollution and energy waste (Wu et al., 2019; Li et al., 2022b; Liu et al., 2022b). Therefore, environmentally-friendly alternative binder materials to substitute Portland cement become increasingly necessary (Jin et al., 2020). Geopolymer, a new type of inorganic aluminosilicate binder with an amorphous or semi-crystalline nature, is frequently used as a replacement for Portland cement to obtain sustainable construction materials (Zheng et al., 2015; Huang et al., 2020; Kumar et al., 2021; Trincal et al., 2022; Zhang et al., 2022a). Geopolymer is a low-carbon cementing material first proposed by Davidovits in the 1970s. It has been reported to exhibit a wide variety of properties for multi-applications, such as cementitious binders (Li et al., 2021), hazardous substance stabilization (Wang et al., 2017; Liu et al., 2022; Lan et al., 2022), fire resistance (Lahoti et al., 2019), wastewater treatment (Rasaki et al., 2019), new building materials (Raza and Zhong, 2022), etc.

Up till now, the development of geopolymers with high early strength and quick hardening has been the research focus of many scholars. The laws of setting and development of early strength for geopolymers can be regulated using fast setting agent, creating appropriate curing conditions, or aggressive chemical treatment. Hassan et al. (2019) verified that curing at high temperature could greatly accelerate the strength development of geopolymer concrete. After curing for several hours at 80–90 °C, the compressive strength can reach about 90% of the maximum strength. Al-Majidi et al. (2016) investigated the influence of curing conditions on the mechanical properties of fly ash-slag geopolymer mortar. Results showed the geopolymer subjected to elevated temperature curing conditions possessed higher early strength than that under ambient conditions at the curing age of 3 d. However, the compressive strength remained almost the same for the heat-cured geopolymer at the curing age of 28 d. Most previous studies about the design of geopolymer mainly focus on excellent mechanical properties at early stages, there are few studies involving the long-term strength and stability of the geopolymers. It is well known that the particle size distribution of the raw materials can greatly affect the density of the internal structure of the geopolymer, which was closely related to its durability properties (Qaidi et al., 2022). In addition, the system's alkalinity greatly impacts the amount of dissolved Si and Al, which can influence the degree of geopolymerization and long-term stability of the geopolymers (Liu et al., 2022a). The durability performance of geopolymer is also one of the key factors to determine whether it can be widely used in industrial applications (Fu et al., 2021; de Oliveira et al., 2022; Gholampour et al., 2022). Therefore, there is urgent need to achieve a balance between the initial and long-term properties of the designed geopolymers under multiple conditions.

Geopolymers are usually fabricated from silica- and alumina-rich source materials. Shell coal gasification fly ash (SFA) and steel slag (SS), as two kinds of industrial solid waste, both possess a certain reactivity for geopolymerization and hydration (Kusiorowski et al., 2021; Zhu et al., 2021; Ma et al., 2022). However, it was reported in our previous studies that there was great difference in particle size, chemical composition and hydration process between the two particles (Chen et al., 2019; Zhou et al., 2022). SFA was richer in amorphous silicon and aluminum than SS, resulting in diverse polymerization processes for the two particles. In addition, the particle size of SFA was much smaller than that of SS. The raw materials with various particle size distributions would result in different mechanical properties at diverse curing ages. More importantly, the mineral composition, microstructure, compactness and alkali content of SFA-based geopolymer and SS-based geopolymer varied from each other, which may lead to differences in the long term properties. To the best of our knowledge, a systematic study on the durability of geopolymers prepared using SFA and SS as raw materials has never been explored.

Herein, we developed a novel technology to provide an effective approach for the materialization of amorphous-rich slags. Two types of geopolymers with high early strength and high final strength respectively were properly designed and successfully synthesized based on SFA and SS. The unconfined compressive strength and flexural strength of the geopolymers were studied. Moreover, long-term stability capabilities of acid-base resistance, freeze–thaw resistance, leaching toxicity, thermal stability, sulfate resistance and carbonation resistance were systematically evaluated. The specific goals were 1) revealing the competition mechanism of geopolymerization and hydration of the amorphous-rich slags based geopolymers by introducing in SS, 2) investigating the long-term stabilization of heavy metals and the durability mechanism, and 3) comparing the mechanical properties and the cost of production of the two geopolymer concrete (GPC), which can provide technical support for promoting the comprehensive utilization of the industrial solid wastes and pave way for the sustainable development in the construction industry.

2 Materials and methods

2.1 Materials

SFA was supplied by Sinopec in Yue Yang, Hunan,

China. SS was converter slag obtained from Baowu Steel Group in Wuhan, Hubei, China. All the SS was ball-milled at 3000 r/min for 40 min by the XQM-4L ball milling machine, and then passed through a 0.075 mm sieve. MK was acquired by calcinating Kaolin with an analytical purity of 99.8% at 750 °C for 1 h. All the above raw materials were dried at 105 °C for 24 h before use. Kaolin, water glass (industrial purity) and sodium hydroxide (analytical purity) were all purchased from Sinopharm Chemical Reagent Co. Ltd. The chemical compositions of raw materials are given in Table 1.

Alkalinity I is defined as the mass ratio of alkaline oxides (Na_2O, K_2O, CaO) and acidic oxides (SiO_2, Al_2O_3, Fe_2O_3) in the ash. The results showed that SFA and SS were alkaline industrial wastes. The content of CaO in steel slag was as high as 45.72%, and the pH value of leaching solution reached 10.32. SFA and SS were both industrial solid wastes, in which trace heavy metals may affect the environment. Accordingly, TCLP method was used to evaluate the heavy metal leaching characteristics, and the results were shown in Fig. S1. It could be seen from Figure S1 that the leaching concentrations of Cd, Mn and Ni in SFA were 5, 10 and 40 times higher than the Class III limit value in the Standard for Groundwater Quality (GB/T 14848-2017), respectively, which may cause environmental risks in the long term service. In contrast, the leaching concentrations of heavy metals in SS and MK were respectively low, so they were suitable as alkali-activated raw materials. The particle sizes of the raw materials were tested using a laser particle size analyzer.

2.2 Synthesis of geopolymer

According to our previous study, two kinds of geopolymers with high early strength and high final strength respectively were successfully synthesized. The geopolymer with the highest long-term unconfined compressive strength (UCS) was named ASK1. The mass ratio of SFA:SS for ASK1 was controlled at 2:1, and 3% of MK was used as the admixture to provide the early strength. The geopolymer with the highest early UCS was named ASK2. The mass ratio of SFA:SS for ASK2 was controlled at 1:10, and 3% of MK was also used as the admixture.

Table 1 Chemical composition of raw materials (%)

Major components	SFA	SS	MK
SiO_2	59.43	11.9	56.09
MgO	2.08	3.16	0.06
Fe_2O_3	2.25	31.85	0.77
Na_2O	1.58	0.03	0.18
CaO	5.17	45.72	0.26
Al_2O_3	20.72	1.23	40.23
K_2O	2.37	0.03	0.16
SO_3	0.2	0.22	0.01
Cl	1.57	0.03	0.02
Leaching pH	8.05	10.32	7.03

The activator mixture was prepared using 31.9% of NaOH solution (Sodium Hydroxide, SH), 53.2% of water glass (Sodium Silicate, SS) and 14.9% of deionized water. The raw materials after drying were mixed according to the designed ratio, and then stirred for 5 min. After that, the alkali-activated solution was added, and the mixture was under continuous stirring for 5–10 min to obtain the precursor. The slurry was placed in a 20 mm × 20 mm × 20 mm mold and cured under different temperatures and humidity. After 24 h of curing, the specimens were demolded for the measurements.

2.3 Analysis methods of geopolymer

2.3.1 Mechanical property test

The UCS and flexural strength (FS) of geopolymers were tested at curing ages of 3, 7, 14, 28 and 60 d (under the curing condition of 23 ± 2 °C with a relative humidity of 65 ± 5%). Specimens having size of 40 mm × 40 mm × 160 mm were subjected to FS test according to the Standard for the Test Method of Cement Mortar Strength (ISO method) (GB/T 17671-2021) with cement electric anti-folding tester (DKZ-5000) at a loading rate of 50 ± 10 N/s. The broken prisms at FS test were then used for UCS tests at a loading rate of 1000 N/s with a universal compression test machine (60 kN max. WEW-300E. Wuxi, China) according to the Standard for Test Method of Basic Properties of Construction Mortar (JGJ/T 70-2009).

2.3.2 Freeze–thaw resistance test

The freeze–thaw resistance of geopolymers mortar samples with dimensions of 20 mm × 20 mm × 20 mm were evaluated using a rapid freeze–thaw cycle test with different freeze–thaw times according to the Standard for Test Methods of Long-term Performance and Durability of Ordinary Concrete (GBT50082-2009). The weight loss and UCS of specimens at 0, 10, 25, 50 and 100 freeze–thaw times were test, respectively. The crushed specimens were broken and sieved through a 0.9 mm mesh, then dried at 60 °C. Next, the dried specimen blocks were immerged in an acetic acid buffer solution (pH = 2.88) with a solid-to-liquid ratio of 50 g/L according to TCLP test. The concentration of the heavy metals in leachates was detected with an inductive coupled plasma mass spectrometer (ICP-MS).

2.3.3 Acid-base and sulfate resistance test

The geopolymer mortar samples with dimensions of

20 mm × 20 mm × 20 mm were cured at 23 ± 2 °C with a relative humidity of 65 ± 5% for 1 d. Subsequently, the specimens were put into HNO_3 solution (with H^+ concentration of 5 wt%), KOH solution (with OH^- concentrations of 5, 10, 15, 20, 15 wt%), 5 wt% sulfate solution ($MgSO_4$, Na_2SO_4, and $Na_2SO_4/MgSO_4$ mix solution) and cured for 5, 30, 45, 60 and 90 d, respectively. All solutions were pre-prepared and renewed every three days. After the acid/base and sulfate exposure, the specimens were taken out and dried at 60 °C. The control sample without soaking were maintained under curing condition of 23 ± 2 °C with a relative humidity of 65 ± 5% for the same duration. After the sulfate exposure, the UCS with and without exposure were measured for UCS loss calculation. The UCS and mass variation of the specimens with and without exposure to acid and base solution after 28 d was used for the evaluation of acid-base resistance performance.

2.3.4 Thermal stability test

The slurry precursor was quickly cast into a mold (20 mm × 20 mm × 20 mm) and sealed to prevent excessive moisture loss and pre-cured in a thermostat at 20, 30, 40, 60 and 90 °C for 24 h with a relative humidity of 90 ± 5%, respectively. After 24 h of pre-curing, the specimens were demolded and re-cured at 23 ± 2 °C with a relative humidity of 65 ± 5% for 28 d. After the secondary curing, the UCS of geopolymers were investigated.

2.4 Characterization of geopolymer

2.4.1 Mineralogical characteristics

The mineral compositions of the obtained samples were characterized by X-ray diffraction (XRD) analysis on D8 advance X-ray diffractometer with filtered Cu Kα radiation (λ (Kα1) = 1.54056 Å, voltage of 40 kV and current of 40 mA) having a scanning speed of 5°/min and diffraction angle from 10° to 80°.

2.4.2 Morphologies and elemental compositions

The morphologies and elemental compositions of the crushed samples (d < 1 mm) were examined using scanning electron microscopy (SEM, JSM-5610LV, magnification ranging from 5000× to 15000×) equipped with an energy-dispersive X-ray (EDX) analyzer after coating with Au for 2 min at 15 mA, 1 mbar.

2.4.3 Thermogravimetric analysis

The $CaCO_3$ or crystal water content of the solid samples obtained from the from thermogravimetry (TG/DTG, STA499c, heated from 30 to 1000 °C at a rate of 10 °C/min under the atmosphere of N_2). The weight loss from 600 to 800 °C corresponded to the decomposition of calcite.

3 Results and discussion

3.1 Mechanical property of geopolymer

The influence of curing age on the UCS and FS of the two kinds of geopolymers was investigated and shown in Fig. 1. The development of UCS for geopolymers was affected by the proportion of raw materials. It could be seen from Fig. 1(a) that the UCS of ASK1 was relatively low at the initial stage, which was only 9.0 MPa after 3 d of curing. However, the UCS of ASK1 increased rapidly thereafter, which could reach 76.6 MPa after 60 d of curing. It was because the geopolymerization process of ASK1 included periodic steps of dissolution, homogeneous nucleation, and heterogeneous growth. The repeated geopolymerization process contributed to the

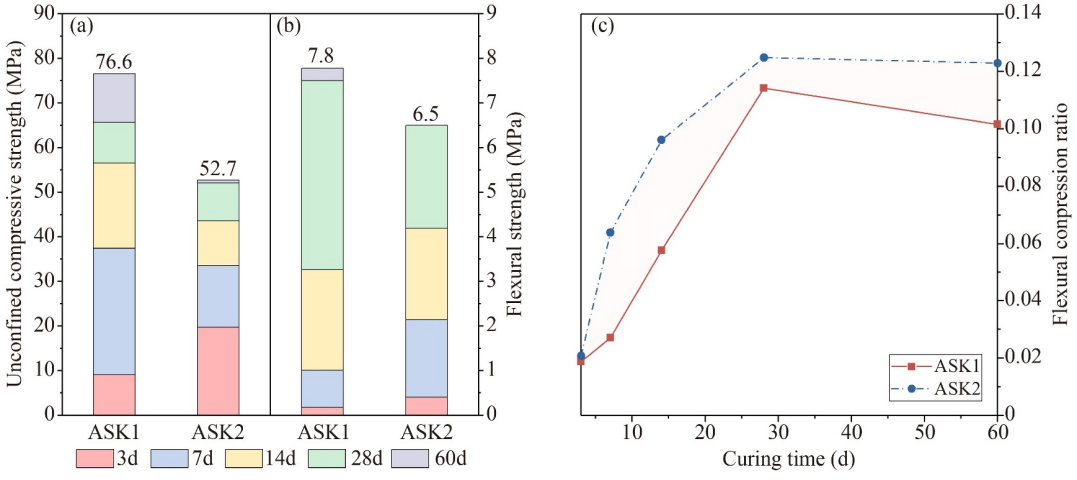

Fig. 1 (a) UCS, (b) FS and (c) Flexural compression ratio of ASK1 and ASK2.

continuous growth of UCS for ASK1 (Zhou et al., 2022). In comparison, ASK2 exhibited high early strength, with UCS close to 20.0 MPa after 3 d of curing. However, the UCS of ASK2 was immediately surpassed by that of ASK1 after curing ages of 5 d. Similar to UCS, FS of ASK1 also developed slowly at initial stage, and increased rapidly at later stage (Fig. 1(b)). Although the initial FS of ASK1 was lower than that of ASK2, the later FS of ASK1 exceeded that of ASK2. Fig. 1(c) indicated that the flexural compression ratio of ASK1 and ASK2 tended to increase as the curing age increased from 5 to 28 d, but began to decrease after 28 d. Studies (Gao et al., 2022) have indicated that Si/Al ratio and microstructure development of geopolymer are determining factors of flexural strength. As the dominant polymerization proceeded in ASK1, Al was consumed, which affected the structural reorientation and resulted in the formation of a small amount of granular geopolymer with higher Si/Al ratio and impeding the flexural strength development (Tang et al., 2022). Therefore, the flexural compression ratio of ASK1 decreased at later curing ages.

The particle size distributions of SFA, SS and MK were presented in Fig. 2(a). It was well known that the Modified Andreasen and Andersen model (MAAM) was widely used to design cement-based materials with an optimized particle packing (Ragalwar et al., 2020; Zhang et al., 2022b), and the model parameters were presented in Eq. (1).

$$P(D_i) = \frac{D_i^q - D_{\min}^q}{D_{\max}^q - D_{\min}^q} \times 100\%, \quad (1)$$

where D_i is the particle size (μm), $P(D_i)$ is the fraction of the total solids smaller than size D_i, $D_{\max}$ is the maximum particle size (μm), $D_{\min}$ is the minimum particle size (μm) and q is the distribution modulus. As recommended in previous literature (Brouwers, 2006), the value of q is fixed at 0.25 in this study.

Here, MAAM acted as a target function for the theoretical optimization of the constitution of the raw materials. The target curve and the cumulative distributions of the dry mixtures were shown in Fig. 2(b). According to the actual situation, an optimization algorithm based on the Least Squares Method (LSM) as presented in Eq. (2) was employed to obtain the mix proportions closest to the target curve.

$$RSS = \sum_{i=1}^{n} [P_{mix}(D_i^{i+1}) - P_{tar}(D_i^{i+1})]^2, \quad (2)$$

where RSS refers to Residual Sum of Squares, P_{mix} and P_{tar} represent the volume distribution of the particle in the mix curve and target curve, respectively.

As could be seen in Fig. 2(b), although ASK2 possessed a larger particle size than ASK1, the cumulative distribution of the dry mixtures for ASK2 was closer to the target curve than that for ASK1. Also, the RSS for ASK2 was calculated to be 4282, which was much smaller than that of ASK1 (18277). The results revealed better packing density of the granular components for ASK2. At initial stage of curing ages when the degree of polymerization was relatively low, the better packing density for ASK2 generally endowed the geopolymer with larger mechanical property. With the increase of curing age, ASK1 showed better mechanical performance than ASK2. It was due to the fact that ASK1 had a higher content of SFA, which was potentially an excellent hydration active material, promoting the strength development for ASK1 at later stage of curing ages when higher polymerization degree was gradually reached.

3.2 Durability of geopolymer

3.2.1 Acid-base resistance

UCS and mass loss of ASK1 and ASK2 under acid and

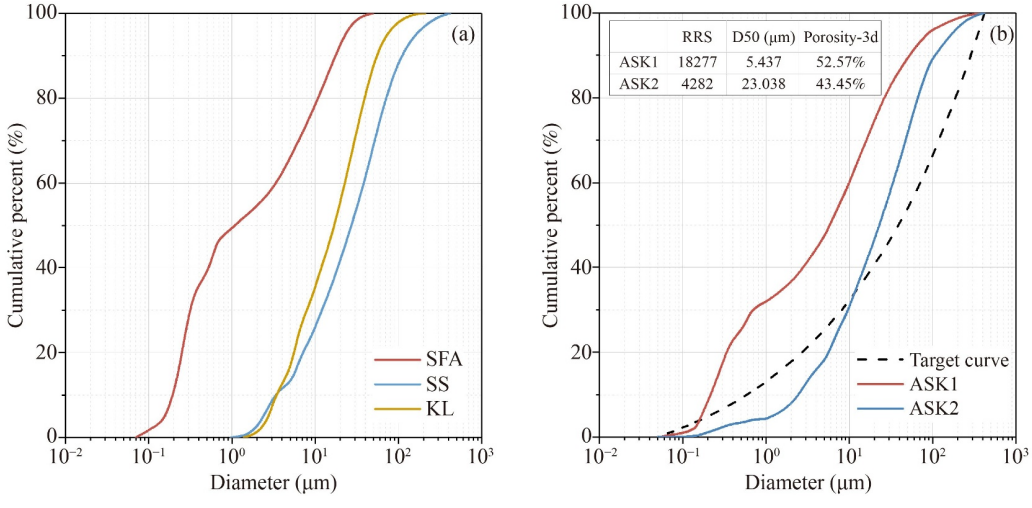

Fig. 2 (a) Particle size distributions of raw materials and (b) the target curve and the cumulative distributions of the dry mixtures.

base corrosion were measured and shown in Fig. 3. For the two geopolymers, the mass loss under HNO_3 corrosion was both less than 10%. It was well known that the bridging oxygen bonding was more vulnerable to H^+ attack in Si-O-Si than that in Si-O-Al (Guo et al., 2016). The oxygen atom in Si-O-Al would be destroyed only when the cation with balanced charge was separated. Therefore, ASK1 had stronger acid corrosion resistance than ASK2 because the Al-O-R content in ASK1 was higher than that in ASK2.

Geopolymer was synthesized via alkali excitation, thus its alkali resistance was better than acid resistance. The UCS of ASK1 increased slowly with the increase of KOH concentration. When the KOH concentration reached 25%, the UCS of ASK1 rose from 64.5 to 68.6 MPa. However, a slight mass loss of ASK1 (less than 0.5%) immersed in 5%–15% KOH was observed. It was because alkali could promote the dissolution of raw material fragments and polymers with low degree of polymerization in ASK1, facilitating the re-polymerization reaction. In addition, a slower growth rate of UCS and a continuous mass loss were found in ASK2. This might be contributed to the high SS content in ASK2. The C_2S and C_3S in SS are more vulnerable to alkali attack (Liu et al., 2021a), leading to decreasing the rate of geopolymerization reactions in the raw materials and the lower UCS growth.

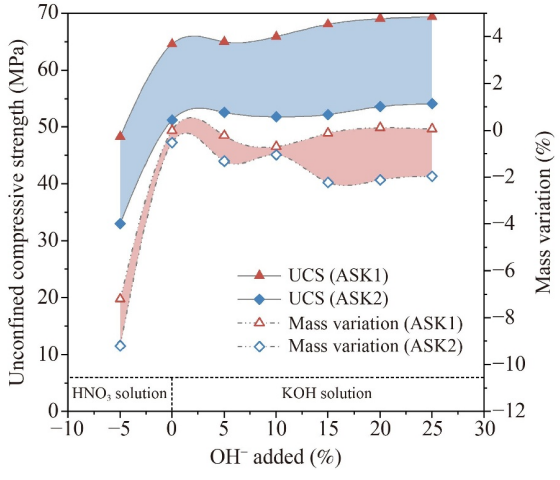

Fig. 3 The acid-base corrosion resistance of ASK1 and ASK2.

3.2.2 Freeze–thaw resistance

The UCS loss and FS loss of the geopolymers at different freezing and thawing cycles were presented in Fig. 4. The loss rates of UCS for ASK1 and ASK2 after 10/25/50/100 freeze–thaw cycles were 3.8%/13.7%/21.4%/48.8% and 8.4%/14.8%/25.7%/51.3%, respectively. The freeze–thaw resistance of ASK1 was better than that of ASK2, with the UCS of ASK1 still reaching 35 MPa after 100 freezing and thawing cycles. As was well known that the polymerization degree of SiO_4 and AlO_4 tetrahedron in the geopolymer was relatively high (Cheng et al., 2018), and the repulsive force between molecules was large, thus making the loss of UCS during freezing and thawing rather small. For ASK2 with a higher content of SS, the loss of UCS was more evident. It was because the hydration products produced by SS were more easily affected by the freezing and thawing cycles. Moreover, for the two geopolymers, the FS loss rate both exceeded 30% after 10 cycles, and exceeded 55% after 100 cycles. Freezing and thawing led to the expansion of free water, destroying the polymer structure (Davidovits, 2017). The reason for the large loss of FS was that the cracks in samples were in parallel with the pressure load, while the damage caused by flexural stress was perpendicular to the pressure load (Aygörmez et al., 2020a).

The leaching concentrations of the heavy metals after 0/10/25/50/100 cycles of freezing and thawing were tested and shown in Fig. 5. There was a sharp decrease in the leaching concentration of heavy metals after

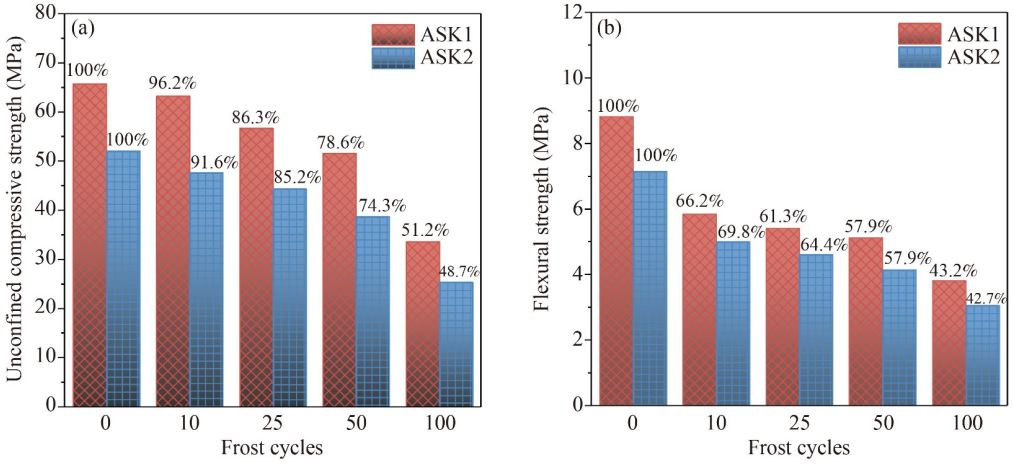

Fig. 4 (a) UCS loss and (b) FS loss of ASK1 and ASK2 at different freezing and thawing cycles.

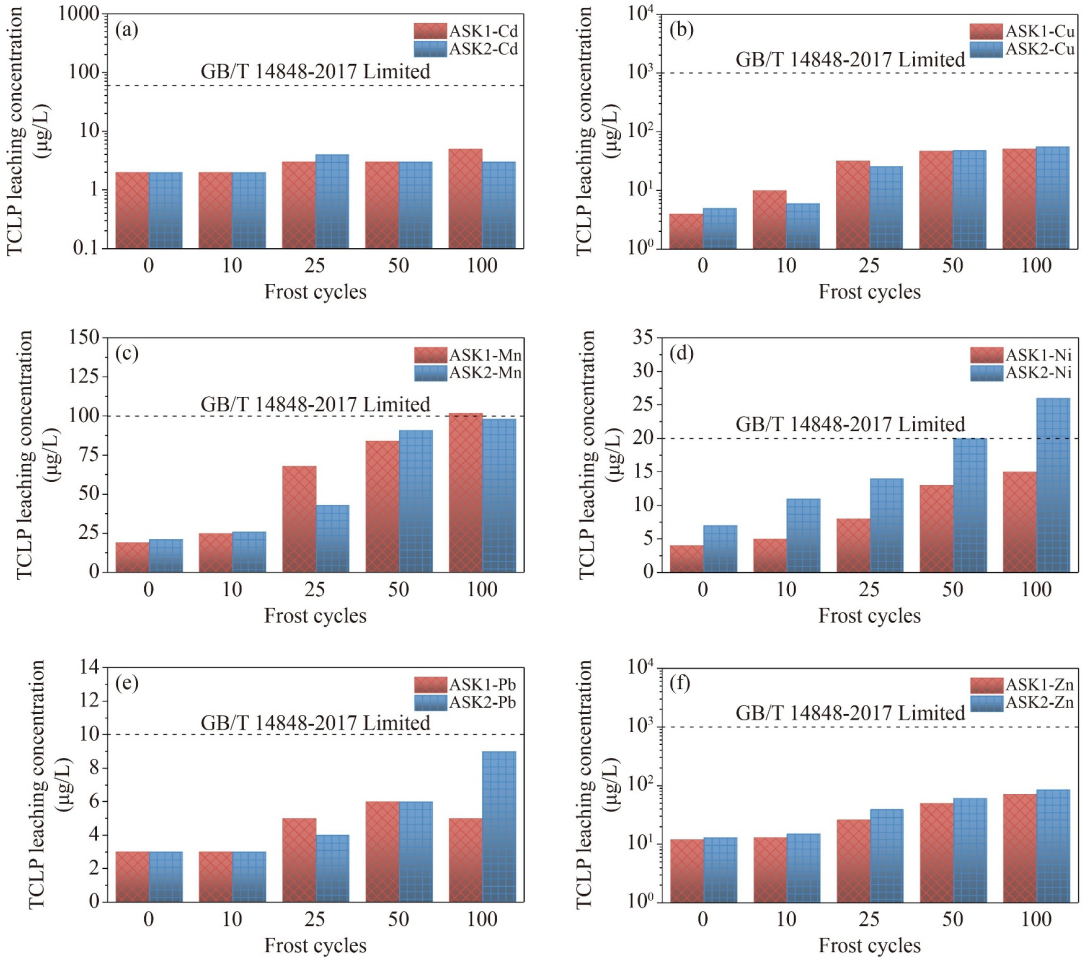

Fig. 5 Leaching concentrations of the heavy metals at different freezing and thawing cycles.

geopolymerization reaction for both ASK1 and ASK2. The heavy metal stabilization efficiency of ASK1 followed the order of Ni (99.2%) > Cd (94.7%) > Cu (93.6%) > Pb (92.8%) > Mn (68.9%) > Zn (65.7%). And the heavy metal stabilization efficiency of ASK2 followed the order of Cu (94.7%) > Ni (94.4%) > Zn (94.2%) > Mn (91.1%) > Pb (83.9%) > Cd (49.5%). After 50 cycles of freezing and thawing, the leaching concentrations of all the heavy metals in the two geopolymers were lower than the standard limit, indicating the long-term stabilization effect on the heavy metals. The leaching concentrations of Mn in ASK1 and Ni in ASK2 only slightly exceeded the standard limit after 100 cycles of freezing and thawing, which had a negligible impact on environment as the toxicity and the ecological risk of these two heavy metals were relatively low.

3.2.3 Thermal stability

The influence of different curing temperatures on the UCS of the two geopolymers was investigated and presented in Fig. 6. During the early period of curing for ASK1, the UCS increased with the increase of temperature from 20 to 60 °C. And there was nearly no change in the UCS when the temperature exceeded 60 °C. It was because the initial reaction mainly included dissolution and polycondensation. In this case, increasing temperature could efficiently increase the rate of polycondensation reaction. However, when the temperature rose to a certain level, the increased water loss could hinder the dissolution of active minerals and slow down the polycondensation process, thus hindering the development of UCS. After 28 d of curing, there was not evident increase of UCS when the temperature ascended. The UCS even decreased when the temperature exceeded 60 °C. It was mainly because polycondensation reaction was completed during the late curing ages. The increase of the temperature may accelerate the dissolution of scattered polymers in alkaline environment and destroy the polymer structure instead (Aygörmez et al., 2020b), leading to the decrease of UCS.

For ASK2 with high early strength, the increase of the curing temperature would prevent the formation of

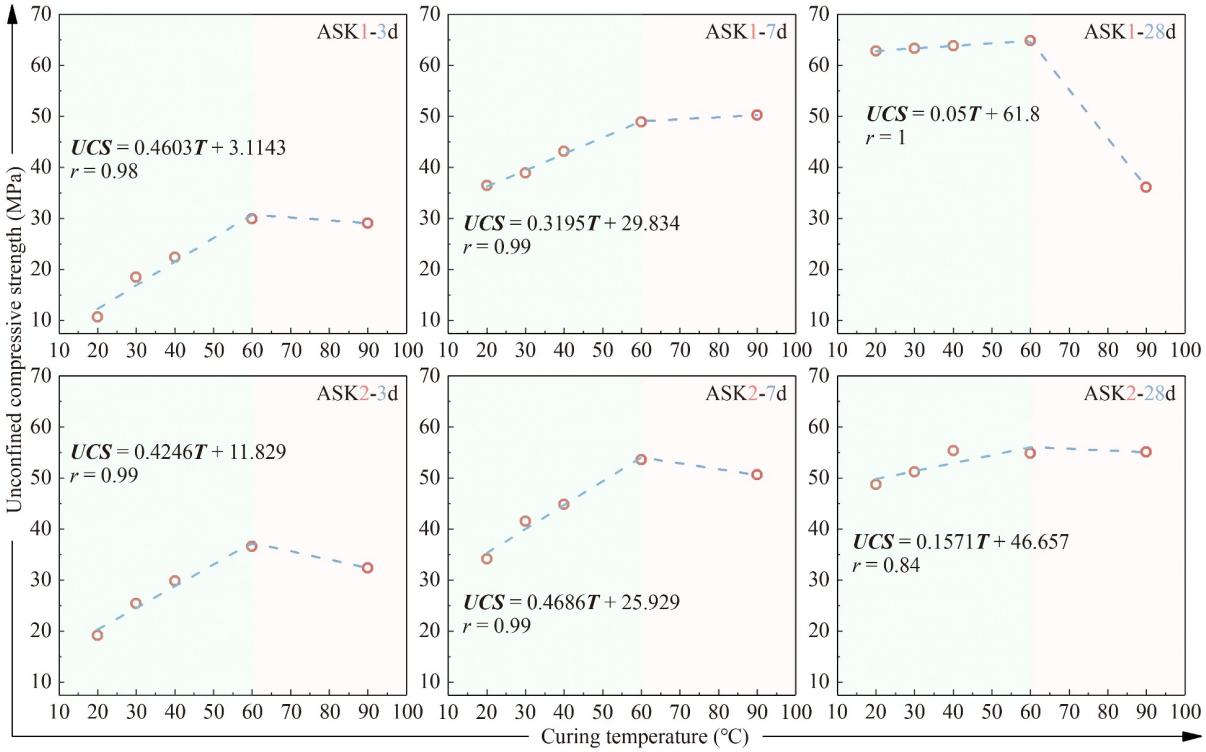

Fig. 6 UCS variation of ASK1 and ASK2 influenced by curing temperature.

hydration products. The UCS started to decline when the temperature exceeded 60 °C at the curing ages of 3 and 7 d. And the UCS started to decline when the temperature exceeded 40 °C at the curing ages of 28 d. The results indicated that the increase of curing temperature could only accelerate polymerization process, but had no obvious effect on the final polymer product.

3.2.4 Sulfate resistance

The influence of sulfate on the UCS of the two geopolymers was investigated and presented in Fig. 7. After immersed in Na_2SO_4, $MgSO_4$ and the mixed solution of Na_2SO_4/$MgSO_4$ for 90 d, the loss rate of UCS for ASK1 was 6.2%, 5.7% and 4.1%, respectively, and the loss rate of UCS for ASK2 was 6.1%, 5.9% and 5.5%, respectively. Both geopolymers showed excellent sulfate corrosion resistance. In Portland cement, sulfate could corrode C-S-H gel, and coprecipitate with Ca^{2+} to generate $CaSO_4$, causing expansion and fragmentation of the cement (Chen et al., 2021). In the geopolymer, however, Na^+, K^+ and Ca^{2+} were harmonic ions for charge balance between interlayers of polymer molecular chains. In this case, the coprecipitation of sulfate and Ca^{2+} had little effect on the structure of the geopolymer.

Among different sulfate solutions, the loss rate of UCS under Na_2SO_4 corrosion was the highest for the two geopolymers. It was because the ionization degree of Na_2SO_4 was higher than that of $MgSO_4$. Additionally, the smaller radius of Na^+ ions endow them with faster diffusion speed and stronger erosion effect. Notably, during the immersion period of 0–15 d, the UCS of the two geopolymers increased by about 4%. It was because at the initial stage of diffusion, Na^+ and Mg^{2+} could enter into the geopolymers to balance the charge, leading to the closer connection between the geopolymer molecules and the improvement of the UCS for the geopolymers.

3.2.5 Carbonation resistance

$CaCO_3$ produced by carbonization could cause expansion and damage to the building material structure (Meek et al., 2021), resulting in the decrease of UCS. According to the weight loss curve in TG-DTG, the content of crystal water in the mineral and the degree of carbonation could be quantitatively analyzed. From the TG-DTG curves of the two geopolymers at the curing age of 60 d (Fig. 8), it could be seen that the weight loss of ASK1 was much less than that of ASK2. For ASK1, little weight loss was observed when the temperature was below 600 °C. The weight loss of 1.2% for ASK1 between 600 and 800 °C was attributed to the $CaCO_3$ decomposition. And the content of $CaCO_3$ was calculated to be 2.73% for ASK1. There were three weight loss ranges for ASK2. The initial weight loss between 100 and 150 °C was caused by the desorption of pore water and surface adsorbed water. The weight loss between 200 and 250 °C was due to the loss of bound water of almandine and

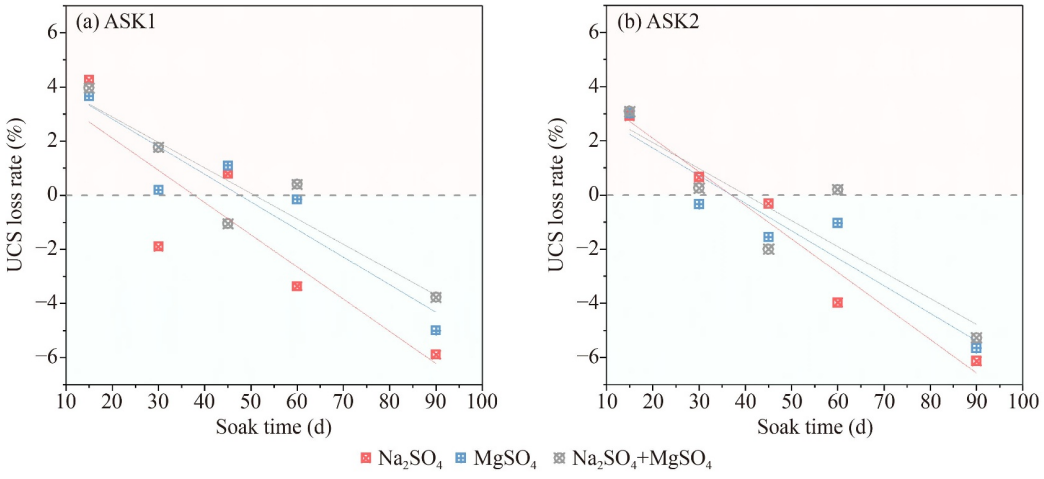

Fig. 7 UCS variation of ASK1 and ASK2 influenced by sulfate.

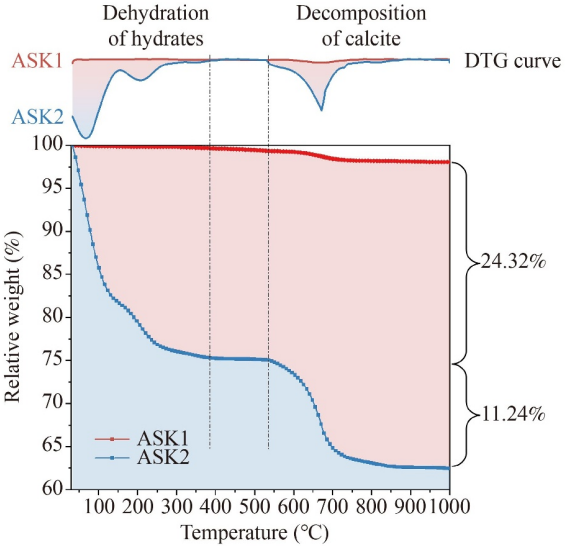

Fig. 8 TG-DTG of ASK1 and ASK2 at the curing age of 60 d.

hydrated calcium aluminate, etc. (Westrum et al., 1979). The weight loss up to 9.3% was observed between 600 and 770 °C, due to the $CaCO_3$ decomposition. And the content of $CaCO_3$ was calculated to be 20.52% for ASK2. The results demonstrated that the carbonation resistance of ASK1 was much higher than that of ASK2. ASK2 had a higher content of SS, which contained a certain amount of f-CaO. Thus it was easier for ASK2 to form the mineral phase containing Ca in alkaline system, endowing it with poorer carbonation resistance. Cations such as Ca^{2+} and Na^{+} in the geopolymers were bound by the negatively charged polymer, providing less chance for the contact between Ca^{2+} and CO_3^{2-} in the liquid phase (Bortnovsky et al., 2008).

3.3 Characterization of geopolymer

3.3.1 XRD analysis

Mineral compositions of ASK1 and ASK2 at curing ages of 3, 28 and 60 d were measured and presented in Fig. 9. A broad peak was found between 18° and 30° for the ASK1 precursor, implying the presence of amorphous silicon and aluminum phases (Chindaprasirt et al., 2022). At the curing age of 3 d, the mineral compositions of ASK1 and ASK2 greatly resembled that of ASK1 precursor. With the increase of curing ages, the position

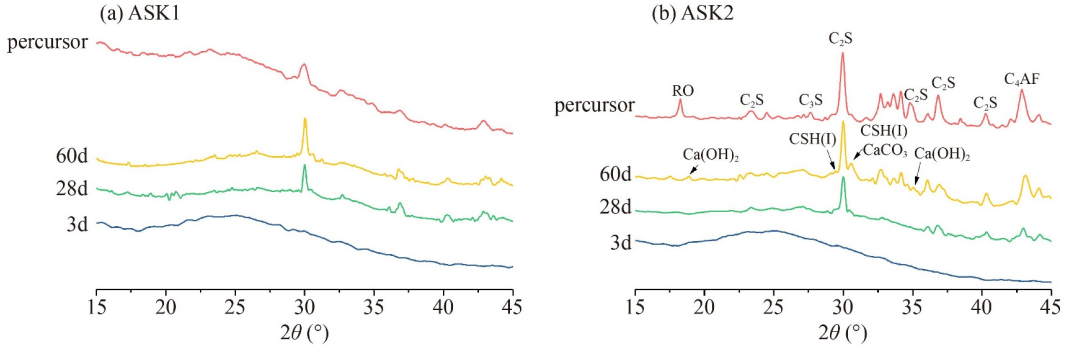

Fig. 9 XRD patterns of ASK1 and ASK2 at diverse curing ages.

of the center of the broad peak gradually shifted toward the higher angle region, implying the occurrence of geopolymerization for the two geopolymers (Silva et al., 2007). It was worth noting that at the curing ages of 60 d, the peaks of C_2S, CSH, $Ca(OH)_2$ and $CaCO_3$ could also be found. The appearance of an amorphous peak at the curing age of 3 d for ASK2 was contributed to the formation of some geopolymer fragments wrapped on the surface of SS particles. With the increase of curing age, the hydration reaction took place at the same time, leading to the emergence of the diffraction peaks of hydration products at the curing age of 60 d for ASK2. Also, the strong alkalinity promoted the formation of $Ca(OH)_2$ and $CaCO_3$. Compared with ASK2 precursor, the diffraction peak of RO was weakened. It was also because the hydration reaction greatly reduced the crystal properties of ASK2 precursor (Bai et al., 2019). Moreover, the obvious diffraction peaks of C_2S at the curing age of 60 d for ASK2 were attributed to the low hydration activity of C_2S (Chang et al., 2021).

3.3.2 SEM/EDX analysis

The morphologies of blended raw materials and geopolymers at different curing ages were shown in Fig. 10. Irregular fragments after alkali corrosion appeared both in ASK1 and ASK2 precursor slurry (Figs. 10(a) and 10(b)). In addition, ASK1 precursor showed some sphere structures, which was attributed to a high content of SFA glass beads. After curing for 3 d, the main structures of ASK1 and ASK2 were formed (Figs. 10(a) and 10(b)). And the more condense structure of ASK2 endowed it with higher early strength. With the increase of curing ages, more integrated surface was formed in ASK1, but there are still some pore with diameter around 1–5 μm distribution in the matrix. At the curing age of 60 d, spherical structures of glass beads completely disappeared in ASK1 (Fig. 10(a)), and a compact layered structure emerged, indicating that polymer molecules were evenly distributed. In contrast, original particle in ASK2 reunited by insufficient faveolate C-S-H, and thus exhibited fragmented morphology (Fig. 10(b)), which led to lower strength of ASK2 during the long-term period. From the element compositions of ASK1 and ASK2 at diverse curing ages (Table S1), it could be found that Ca/Si for ASK2 remained almost the same (Fig. 10(d)). However, Si/Al for ASK1 ascended from 1.32 to 1.52 as the curing age increased from 3 d to 60 d (Fig. 10(c)), implying that amorphous poly-sialate conversion (Li et al., 2022a) and a more stable structure was synthesized (Scheme 1). The results further verified higher long-term strength and better of durability of ASK1.

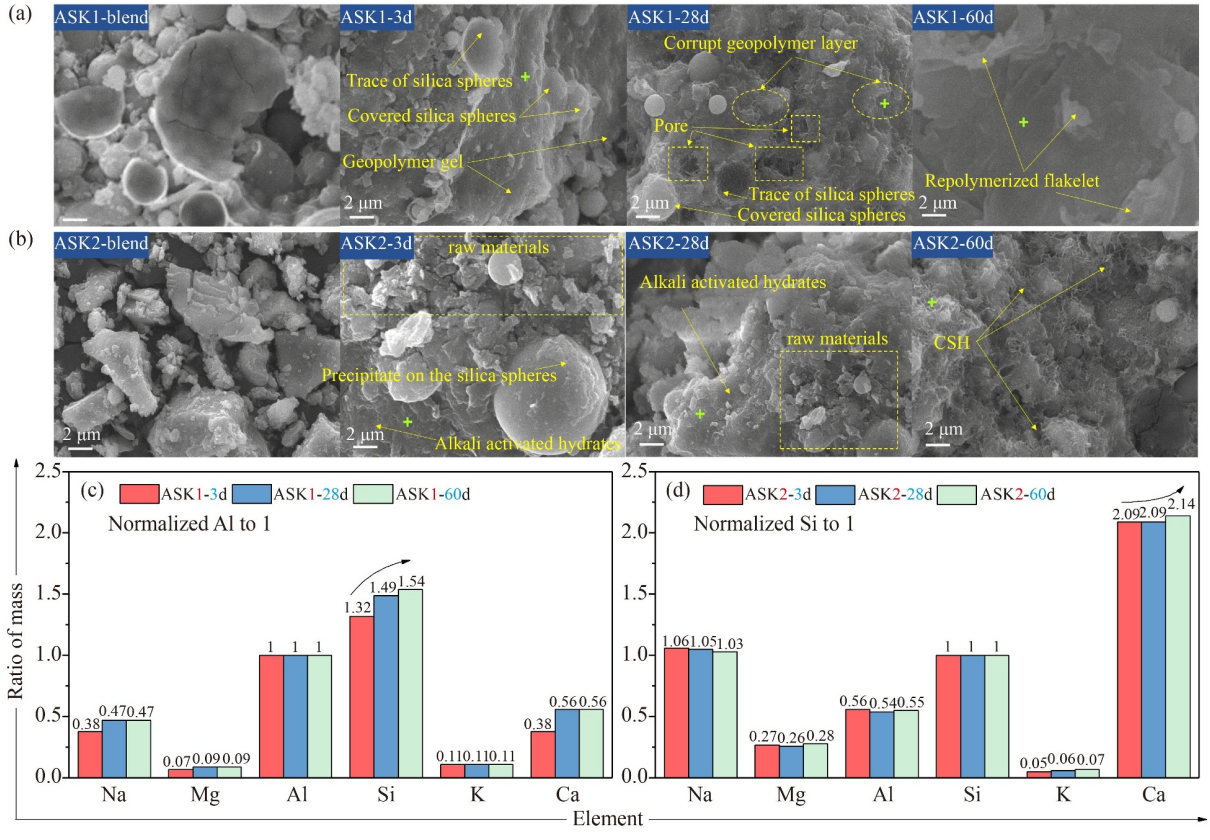

Fig. 10 Microstructures of blended raw materials and geopolymers at diverse curing ages.

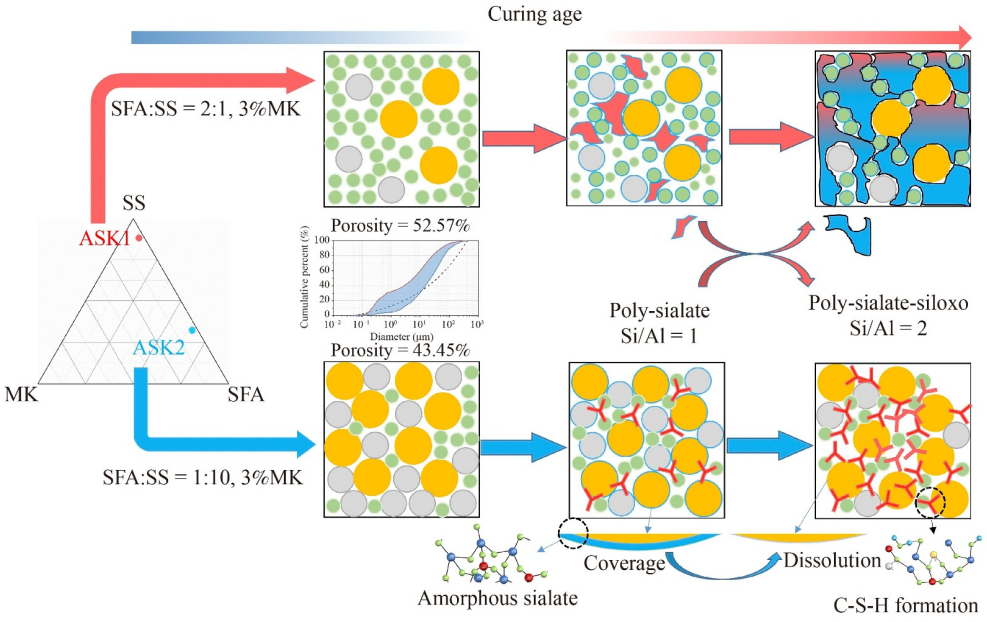

Scheme 1 Mechanism of geopolymerization and hydration.

3.4 Economic assessment of geopolymer paste and concrete

The cost of producing the geopolymer paste and concrete were estimated and presented in Fig. 11. Details of quantity and cost of items involved in the production of different geopolymer paste and concrete were listed in Table S2. The cost of two geopolymer pastes (ASK1 and ASK2) and their concretes (ASK1C and ASK2C) were ¥755.95, ¥793.64, ¥306.83 and ¥314.88, respectively. The total costs of about 36.38%–37.33% were contributed by the alkali activators (SH and SS) to geopolymer paste production. Sodium carbonate, as a more environmentally friendly and economical alkali activators (Adesina, 2021; Oyebisi et al., 2022), may be used to replace SH and SS used in future study to reduce the higher cost arising from the alkali-activation process. In addition, this geopolymer paste could be used in Pb, Cr and Zn immobilization and possessed excellent immobilization efficiency in early-age (Chen et al., 2022), thus has great potential applications for hazardous wastes disposal.

Significantly, there were about 59.98%–61.01% total cost reduction in ASK1C and ASK2C than Portland cement concrete of C30 grade (¥786.85/m^3) (Oyebisi et al., 2022). Due to the energy consumption of SS ball-milling, the cost of concrete ASK2C was 4.99 percent higher than the ASK1C. The cost of ASK2C could be further reduced by shortening the ball-milling time of SS and using its coarse part replacing the Sand/Fine Aggregate in concrete production. In addition to the cost benefits, the geopolymer concrete may facilitate the waste management and commercialization of shell coal gasification fly ash and steel slag, and thus conserving the natural resources and reducing the CO_2 emission.

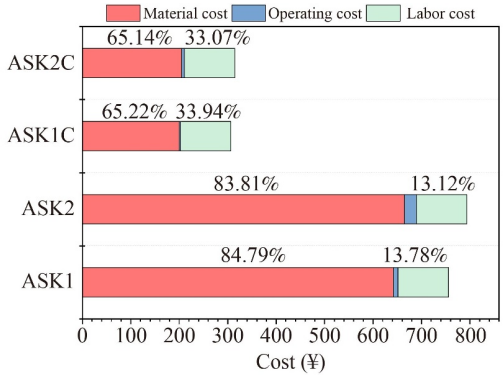

Fig. 11 Contribution of materials, operating, and labor in total cost.

4 Conclusions

1) ASK2 possessed better packing density of the granular components, resulting in a higher early physical strength when the degree of polymerization was relatively low. ASK1 had a larger content of SFA with great pozzolanic activity, leading to a better integrity and higher long-term physical strength.

2) Properly raising the curing temperature could increase the early strength, but had almost no effect on the late strength. Nevertheless, further raising the curing temperature would hinder the development of late strength. Both ASK1 and ASK2 had excellent acid-base resistance and sulfate resistance. The freeze–thaw

resistance, and carbonation resistance of ASK1 were better than that of ASK2. The synthesized ASK1 had stronger long-term stability.

3) Heavy metals in raw materials could be effectively stabilized through geopolymerization process. Except that the leaching concentrations of Mn in ASK1 and Ni in ASK2 slightly exceeded the standard limit, the leaching concentrations of all the other heavy metals after 100 cycles of freezing and thawing met the requirements of corresponding standards. The results of this study could offer a new approach to solidification and stabilization of heavy metals using SFA-SS geopolymers and explore a new way for the comprehensive utilization of industrial solid wastes.

Acknowledgements This research was funded by the Jiangxi Academy of Water Science and Engineering Open Project Fund (No. 2021SKSG04); the National Natural Science Foundation of China (No. 51979011); the Central Non-Profit Scientific Research Fund for Institutes (Nos. CKSF2021483/CL, CKSF2023359/HL, and CKSF2023397/HL); the Knowledge Innovation Program of Science and Technology Bureau of Wuhan, China (No. CKSD2022360/CL).

Conflict of Interest The authors declare that the research was conducted in the absence of any commercial or financial relationships that could be construed as a potential conflict of interest.

Electronic Supplementary Material Supplementary material is available in the online version of this article at https://doi.org/10.1007/s11783-023-1750-9 and is accessible for authorized users.

References

Adesina A (2021). Performance and sustainability overview of sodium carbonate activated slag materials cured at ambient temperature. Resources,. Environment and Sustainability, 3: 100016

Al-Majidi M H, Lampropoulos A, Cundy A, Meikle S (2016). Development of geopolymer mortar under ambient temperature for *in situ* applications. Construction & Building Materials, 120: 198–211

Aygörmez Y, Canpolat O, Al-Mashhadani M M (2020a). Assessment of geopolymer composites durability at one year age. Journal of Building Engineering, 32: 101453

Aygörmez Y, Canpolat O, Al-Mashhadani M M, Uysal M (2020b). Elevated temperature, freezing-thawing and wetting-drying effects on polypropylene fiber reinforced metakaolin based geopolymer composites. Construction & Building Materials, 235: 117502

Bai T, Song Z, Wang H, Wu Y, Huang W (2019). Performance evaluation of metakaolin geopolymer modified by different solid wastes. Journal of Cleaner Production, 226: 114–121

Bortnovsky O, Dědeček J, Tvarůžková Z, Sobalík Z, Šubrt J (2008). Metal ions as probes for characterization of geopolymer materials. Journal of the American Ceramic Society, 91(9): 3052–3057

Brouwers H J H (2006). Particle-size distribution and packing fraction of geometric random packings. Physical Review E: Statistical, Nonlinear, and Soft Matter Physics, 74(3): 031309

Chang J, Jiang T, Cui K (2021). Influence on compressive strength and CO_2 capture after accelerated carbonation of combination β-C_2S with γ-C_2S. Construction & Building Materials, 312: 125359

Chen K, Wu D, Xia L, Cai Q, Zhang Z (2021). Geopolymer concrete durability subjected to aggressive environments: a review of influence factors and comparison with ordinary Portland cement. Construction & Building Materials, 279: 122496

Chen Y, Chen F, Zhou F, Lu M, Hou H, Li J, Liu D, Wang T (2022). Early solidification/stabilization mechanism of heavy metals (Pb, Cr and Zn) in Shell coal gasification fly ash based geopolymer. Science of the Total Environment, 802: 149905

Chen Y, Zhou X, Wan S, Zheng R, Tong J, Hou H, Wang T (2019). Synthesis and characterization of geopolymer composites based on gasification coal fly ash and steel slag. Construction & Building Materials, 211: 646–658

Cheng Y, Hongqiang M, Hongyu C, Jiaxin W, Jing S, Zonghui L, Mingkai Y (2018). Preparation and characterization of coal gangue geopolymers. Construction & Building Materials, 187: 318–326

Chindaprasirt P, Jitsangiam P, Rattanasak U (2022). Hydrophobicity and efflorescence of lightweight fly ash geopolymer incorporated with calcium stearate. Journal of Cleaner Production, 364: 132449

Davidovits J (2017). Geopolymers: ceramic-like inorganic polymers. Journal of Ceramic Science and Technology, 8(3): 335–350

de Oliveira L B, de Azevedo A R G, Marvila M T, Pereira E C, Fediuk R, Vieira C M F (2022). Durability of geopolymers with industrial waste. Case Studies in Construction Materials, 16: e00839

Fu Q, Xu W, Zhao X, Bu M, Yuan Q, Niu D (2021). The microstructure and durability of fly ash-based geopolymer concrete: a review. Ceramics International, 47(21): 29550–29566

Gao B, Jang S, Son H, Park S, Lee H S, Bae C J (2022). Phase transformation and microstructure evolution of a kaolin-based precursor. Ceramics International, 48(24): 36066–36075

Gholampour A, Danish A, Ozbakkaloglu T, Yeon J H, Gencel O (2022). Mechanical and durability properties of natural fiber-reinforced geopolymers containing lead smelter slag and waste glass sand. Construction & Building Materials, 352: 129043

Guo C M, Wang K T, Liu M Y, Li X H, Cui X M (2016). Preparation and characterization of acid-based geopolymer using metakaolin and disused polishing liquid. Ceramics International, 42(7): 9287–9291

Hassan A, Arif M, Shariq M (2019). Use of geopolymer concrete for a cleaner and sustainable environment: a review of mechanical properties and microstructure. Journal of Cleaner Production, 223: 704–728

Huang T, Zhou L, Chen L, Liu W, Zhang S, Liu L (2020). Mechanism exploration on the aluminum supplementation coupling the electrokinetics-activating geopolymerization that reinforces the solidification of the municipal solid waste incineration fly ashes. Waste Management (New York, N.Y.), 103: 361–369

Jin Y, Feng W, Zheng D, Dong Z, Cui H (2020). Structure refinement of fly ash in connection with its reactivity in geopolymerization. Waste Management (New York, N.Y.), 118: 350–359

Kumar N, Amritphale S S, Matthews J C, Lynam J G, Alam S, Abdulkareem O A (2021). Synergistic utilization of diverse industrial wastes for reutilization in steel production and their geopolymerization potential. Waste Management (New York, N.Y.), 126: 728–736

Kusiorowski R, Gerle A, Dudek K, Związek K (2021). Application of hard coal combustion residuals in the production of ceramic building materials. Construction & Building Materials, 304: 124506

Lahoti M, Tan K H, Yang E H (2019). A critical review of geopolymer properties for structural fire-resistance applications. Construction & Building Materials, 221: 514–526

Lan T, Meng Y, Ju T, Chen Z, Du Y, Deng Y, Song M, Han S, Jiang J (2022). Synthesis and application of geopolymers from municipal waste incineration fly ash (MSWI FA) as raw ingredient: a review. Resources, Conservation and Recycling, 182: 106308

Li J, Mailhiot S, Kantola A M, Niu H, Sreenivasan H, Telkki V V, Kinnunen P (2022a). Longitudinal single-sided NMR study: silica-to-alumina ratio changes the reaction mechanism of geopolymer. Cement and Concrete Research, 160: 106921

Li J, Tao Y, Zhuang E, Cui X, Yu K, Yu B, Boluk Y, Bindiganavile V, Chen Z, Yi C (2022b). Optimal amorphous oxide ratios and multifactor models for binary geopolymers from metakaolin blended with substantial sugarcane bagasse ash. Journal of Cleaner Production, 377: 134215

Li Z, Fei M E, Huyan C, Shi X (2021). Nano-engineered, fly ash-based geopolymer composites: an overview. Resources, Conservation and Recycling, 168: 105334

Liu H, He H, Li Y, Hu T, Ni H, Zhang H (2021a). Coupling effect of steel slag in preparation of calcium-containing geopolymers with spent fluid catalytic cracking (FCC) catalyst. Construction & Building Materials, 290: 123194

Liu J, Doh J H, Dinh H L, Ong D E L, Zi G, You I (2022a). Effect of Si/Al molar ratio on the strength behavior of geopolymer derived from various industrial waste: a current state of the art review. Construction & Building Materials, 329: 127134

Liu K, Guan X, Li C, Zhao K, Yang X, Fu R, Li Y, Yu F (2022). Global perspectives and future research directions for the phytoremediation of heavy metal-contaminated soil: a knowledge mapping analysis from 2001 to 2020. Frontiers of Environmental Science & Engineering, 16(6): 73

Liu Z, Deng P, Zhang Z (2022b). Application of silica-rich biomass ash solid waste in geopolymer preparation: a review. Construction & Building Materials, 356: 129142

Ma F, Zhou L, Luo Y, Wang J, Ma B, Qian B, Zang J, Hu Y, Ren X (2022). The mechanism of pristine steel slag for boosted performance of fly ash-based geopolymers. Journal of the Indian Chemical Society, 99(8): 100602

Meek A H, Beckett C T S, Elchalakani M (2021). Reinforcement corrosion in cement- and alternatively-stabilised rammed earth materials. Construction & Building Materials, 274: 122045

Oyebisi S, Olutoge F, Kathirvel P, Oyaotuderekumor I, Lawanson D, Nwani J, Ede A, Kaze R (2022). Sustainability assessment of geopolymer concrete synthesized by slag and corncob ash. Case Studies in Construction Materials, 17: e01665

Qaidi S M A, Sulaiman Atrushi D, Mohammed A S, Unis Ahmed H, Faraj R H, Emad W, Tayeh B A, Mohammed Najm H (2022). Ultra-high-performance geopolymer concrete: a review. Construction & Building Materials, 346: 128495

Ragalwar K, Heard W F, Williams B A, Ranade R (2020). Significance of the particle size distribution modulus for strain-hardening-ultra-high performance concrete (SH-UHPC) matrix design. Construction & Building Materials, 234: 117423

Rasaki S A, Bingxue Z, Guarecuco R, Thomas T, Minghui Y (2019). Geopolymer for use in heavy metals adsorption, and advanced oxidative processes: a critical review. Journal of Cleaner Production, 213: 42–58

Raza M H, Zhong R Y (2022). A sustainable roadmap for additive manufacturing using geopolymers in construction industry. Resources, Conservation and Recycling, 186: 106592

Silva P D, Sagoe-Crenstil K, Sirivivatnanon V (2007). Kinetics of geopolymerization: role of Al_2O_3 and SiO_2. Cement and Concrete Research, 37(4): 512–518

Tang J, Ji X, Liu X, Zhou W, Chang X, Zhang S (2022). Mechanical and microstructural properties of phosphate-based geopolymers with varying Si/Al molar ratios based on the sol-gel method. Materials Letters, 308: 131178

Trincal V, Multon S, Benavent V, Lahalle H, Balsamo B, Caron A, Bucher R, Diaz Caselles L, Cyr M (2022). Shrinkage mitigation of metakaolin-based geopolymer activated by sodium silicate solution. Cement and Concrete Research, 162: 106993

Wang C, Zhu Y, Yao D, Chen G, Wang L (2017). Assessing human bioaccessibility of trace contaminants in size-fractionated red mud, derived precipitates and geopolymeric blocks. Frontiers of Environmental Science & Engineering, 11(6): 12

Westrum E F, Essene E J, Perkins D (1979). Thermophysical properties of the garnet, grossular: $Ca_3Al_2Si_3O_{12}$. Journal of Chemical Thermodynamics, 11(1): 57–66

Wu Y, Lu B, Bai T, Wang H, Du F, Zhang Y, Cai L, Jiang C, Wang W (2019). Geopolymer, green alkali activated cementitious material: sSynthesis, applications and challenges. Construction & Building Materials, 224: 930–949

Zhang B, Yu T, Deng L, Li Y, Guo H, Zhou J, Li L, Peng Y (2022a). Ion-adsorption type rare earth tailings for preparation of alkali-based geopolymer with capacity for heavy metals immobilization. Cement and Concrete Composites, 134: 104768

Zhang W, Zheng M, Zhu L, Lv Y (2022b). Mix design and characteristics evaluation of high-performance concrete with full aeolian sand based on the packing density theory. Construction & Building Materials, 349: 128814

Zheng L, Wang W, Qiao W, Shi Y, Liu X (2015). Immobilization of Cu^{2+}, Zn^{2+}, Pb^{2+}, and Cd^{2+} during geopolymerization. Frontiers of Environmental Science & Engineering, 9(4): 642–648

Zhou X, Chen Y, Dong S, Li H (2022). Geopolymerization kinetics of steel slag activated gasification coal fly ash: a case study for amorphous-rich slags. Journal of Cleaner Production, 379: 134671

Zhu X, Li W, Du Z, Zhou S, Zhang Y, Li F (2021). Recycling and utilization assessment of steel slag in metakaolin based geopolymer from steel slag by-product to green geopolymer. Construction & Building Materials, 305: 124654